Electrochemical characteristics of various Ni-P composite coatings in 0.6M NaCl solution

Mahboobeh Azadi*, Hossein Tavakoli, Saeid Haghighatkhah, Freshteh Amjadi Eranegh

Faculty of Materials and Metallurgical Engineering, Semnan University, Semnan, Iran, P.O. Box: 35131-19111

*Corresponding Author, Email Address: m.azadi@semnan.ac.ir, Phone Number: +98-910-226-0629

Abstract

In this paper, various Ni-P composite coatings containing toner, MoS_2, and nano-SiO_2 particles were deposited on steel substrates by the electroless method. Then, the electrochemical properties of these coatings after a heat treatment process were compared. The microstructural evaluations were also done by using the optical and electron microscopy methods. Both Tafel polarization and electrochemical impedance spectroscopy techniques were utilized to survey the electrochemical behavior of such coatings. The surface morphology of all coatings contained cauliflower-like nodules. The X-ray diffraction patterns showed the crystalline phases of Ni and Ni_3P for all coatings after the heat-treatment step. Obtained results showed that all composite coatings exhibited lower corrosion rates with respect to Ni-P coatings. Such a reduction was about 21.6-92.2%. This behavior was attributed to the presence of reinforcement as barriers for corrosive ion diffusion through the coating plus the changes in detected phases and thickness. Electrochemical impedance spectroscopy test results also demonstrated that the increase in the polarization resistance for composites coatings was about 18.4-85.3% after 1 h immersion in a 0.6M NaCl solution; however, when the immersion time increased to 24 h, such increased resistance changed to 18.1 to 73.1%. Totally, despite the lower deposition rate, the presence of MoS_2 and nano-SiO_2 particles were more effective than toner particles to raise the corrosion rate of the Ni-P coating.

Keyword: Ni-P-MoS_2-SiO_2 nano-composite coatings, Ni-P-MoS_2 composite coatings, Ni-P-Toner composite coatings, Electrochemical properties, Electroless.

Preprints (www.preprints.org) | NOT PEER-REVIEWED | Posted: 26 October 2020 doi:10.20944/preprints202010.0525.v1

1. Introduction

Ni and Ni-based alloys as bulk materials or coatings exhibit high corrosion resistance characteristics in severe conditions. Thus, they are mainly used for chemical, oil, and gas, automotive, electronics, aerospace, and power industries [1-3].

Since the last few decades, the electroless Ni-P coatings, as well as other Ni-based alloys, showed high wear and abrasion resistance, corrosion, and oxidation resistance [4, 5]. The electroless technique as an available and economical method is a free-external current process in which nickel ion is deposited through reducing agents [6]. Besides, to improvement of the Ni-P coatings properties such as hardness, tribological and corrosion resistance additional reinforcement particles like as CeO_2 [1], TiC [3], SiO_2 [7], TiO_2 [8], TiN [9], TaC [10], and ZnO [11] are added to the matrix. These ceramic particles were hard and act as abrasive agent; however, other particles such as graphite, h-BN, MoS_2, WS_2, graphene, and poly-tetra-fluoro-ethylene (PTFE) particles as self-lubricating agents are added to theses coatings to reduce the coefficient of friction of Ni-P coatings [2, 7, 10]. Thus, in some research both types of particles are added to the Ni-P matrix as follows:

Du et al. [12] deposited the Ni-P coatings with $Ti_3C_2T_x$, TiO_2, and MoS_2 particles as reinforcement agents. Their results showed that a mixture of soft and ceramic particles results in the improvement of micro-hardness and corrosion resistance of the Ni-P coatings. This behavior was due to changes in surface roughness and hydrophobicity of coating in the presence of reinforcements. Sharma et al. [13] studied the wear and corrosion characteristics of the electroless Ni-P-PTFE-Al_2O_3 coatings after various heat treatment procedures. The obtained results demonstrated that the corrosion rates for these coatings in 0.6M NaCl decreased when the temperature of heat treatment was not high. Wu et al. [14] made the heat-treated Ni-P-PTFE-SiC composite coatings by the electroless method. These coatings exhibited high micro-hardness and wear resistance with a low friction coefficient. Ping et al. [15] fabricated Ni-P-MoS_2-Al_2O_3 composite coatings without using surfactants. The tribological performance of these coatings was done by a WC ball. They depicted that when both reinforcements added to the Ni-P coatings the surface morphology, coefficient of friction, and wear rate of the fabricated coatings were affected. Mayanglambam et al. [16] investigated the properties of the Ni-P coatings reinforced with pulverized fly ash (PFA) as waste particles. Their results showed that the composite coatings exhibited a higher micro-

Preprints (www.preprints.org) | NOT PEER-REVIEWED | Posted: 26 October 2020 doi:10.20944/preprints202010.0525.v1

hardness when the particles were distributed uniformly in the matrix. Eranegh et al. [7] deposited various Ni-P-SiO_2-MoS_2 coatings and then studied the tribological behavior of coatings. The results showed that both reinforcements raised the micro-hardness and wear resistance of composite coatings.

Thus, the purpose of this paper is to figure out the behavior of Ni-P coatings reinforced by toner, MoS_2, and nano-SiO_2 particles. Then, the microstructural evaluations were done through both field emission scanning electron microscopy (FESEM) and optical microscopy (OM) images. The phase-detection was performed by the X-ray diffraction (XRD) method. Then, both Tafel polarization and the electrochemical impedance spectroscopy (EIS) were applied to survey the electrochemical characteristics of fabricated coatings.

2. Experimental parts

2.1. Coating process

The utilized substrates for various coatings were carbon steel st37. Before the coating deposition, substrates were polished by SiC papers up to 2500 grades, degreased by ethanol and alkaline solution for 1 min. Then, substrates were placed in an acid pickling bath (50% HCl solution) for a few seconds. The chemical composition of the Ni-P bath contained $NiSO_{4.6}H_2O$ (50 g/L), $NaH_2PO_2.H_2O$(25 g/L), $C_6H_5Na_3O_7.2H_2O$ (60 g/L), and CH_3COONH_4 (40 g/L). The bath temperature was about 83-87 °C. The pH of the bath was kept at 4.8 with adding ammonia. More details of the deposition process were found in the previous study [7].

Table 1. Details of all prepared coatings

Coatings name	Reinforcement concentration in bath (g/L)	Reinforcement type
Ni-P	0	0
Ni-P-10M-10S	10, 10	MoS_2, SiO_2
Ni-P-10M-20S	10, 20	MoS_2, SiO_2
Ni-P-1T	1	Toner
Ni-P-2.5T	2.5	Toner

Preprints (www.preprints.org) | NOT PEER-REVIEWED | Posted: 26 October 2020 doi:10.20944/preprints202010.0525.v1

To fabricate other composite coatings with reinforcement, various particles were added to the Ni-P bath with details reported in Table1. It was noticeable that the toner particles were waste material that contained carbonic and oxide groups [17]. The coating process time for all coatings was about 90 mins. To improve the dispersion of particles in the bath, using surfactants and continuous stirring of the bath were done. At last, all coatings were heated at 400 °C for 60 mins. In this situation, the mechanical, physical, and corrosion properties of coatings would be improved through the crystalline structure [4].

2.2. Coating characterization

The surface morphology of various coatings was evaluated by field-emission scanning electron microscopy (FESEM-MIRA3-TSCAN model) and optical microscopy (OM-Olympus model) methods. The phase-detection of the fabricated coatings was determined by an X-ray diffractometer (XRD-Bruker model) with Cu-Kα radiation. The scanning angle was between 10 to 90°. To detect the possible existence bonding energy of toner particle, a Transmittance Fourier-transform infrared spectroscopy (FTIR-Shimadzu model) method were applied. The wavenumber in this test was from 400 to 4000 cm^{-1}.

Both Tafel polarization and EIS tests were applied for evaluations of corrosion properties of various coatings. All electrochemical tests were carried out with a standard three-electrode system in a 0.6M NaCl solution (pH=6.8). The fabricated coatings, saturated calomel electrode (SCE), platinum sheet were utilized as working, reference, and counter electrodes, respectively. These measurements were done at 25 °C. Immersion times for EIS measurements were 1 and 24 h and the range of applied frequency was from 10^5 to 10^{-2} Hz. The increase in the corrosion resistance (R) would be calculated due to equation (1) and (2) based on the polarization and EIS test results, respectively [18, 19],

$$R = \frac{i_{corr(0)} - i_{corr}}{i_{corr(0)}} \times 100 \quad (1)$$

$$R = \frac{R_p - R_{p(0)}}{R_p} \times 100 \quad (2)$$

Preprints (www.preprints.org) | NOT PEER-REVIEWED | Posted: 26 October 2020 doi:10.20944/preprints202010.0525.v1

Where i_{corr} and $i_{corr(0)}$ are the corrosion current density for composites coatings and the Ni-P coating, respectively. Besides, R_p and $R_{p(0)}$ are the polarization resistance for composites coatings and the Ni-P coating, respectively. The EIS plots were analyzed by using Z-view software through the equivalent circuit models. More details of electrochemical measurements were found in previous studies [18, 19].

3. Results and discussion

3.1. FTIR analysis

Figure 1 shows the related pattern of the FTIR test result for toner particles as one of the utilized reinforcement agents.

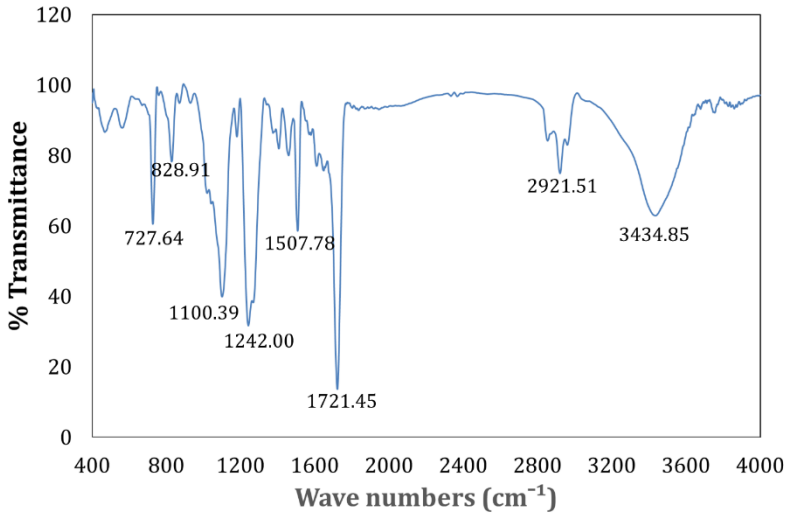

Figure 1. The FTIR test result for toner particles

The wavenumber of 727.64 cm^{-1} was related to the CH_2 bonds as alkanes groups. Besides, it was found that the anti-symmetric CH_2 stretching bonds in the wax material also show a peak at the wavenumber of 2921.51 cm^{-1}. The highest peak (1721.45 cm^{-1}) was related to the C=O stretching bond. The peak of 1100.39 cm^{-1} has corresponded to the Si-O stretching bond. It was found that the O-Fe stretching bond showed a broad peak at the wavenumber of 3434.85 cm^{-1} and peaks at the range of 500-700 cm^{-1}. It was reported that this peak was attributed to the Fe_3O_4 compound [20]. The peak of 1507.78 cm^{-1} was related to the aromatic ring of the C=C stretching bond. It was reported that a peak of 1242 cm^{-1} could be attributed

Preprints (www.preprints.org) | NOT PEER-REVIEWED | Posted: 26 October 2020 doi:10.20944/preprints202010.0525.v1

to the C-O-C stretching bond that showed the esters group [21]. Thus, totally the toner particles contained carbonic groups, silica and Fe_3O_4 compound which was similar to other research [17]. It was found that toner basically consisted of carbon compounds such as paraffin wax, and polypropylene, iron dioxides, silica, surfactants, and other additives [22].

3.2. Microstructural evaluations

Figure 2 shows the OM images from the top section of various coatings.

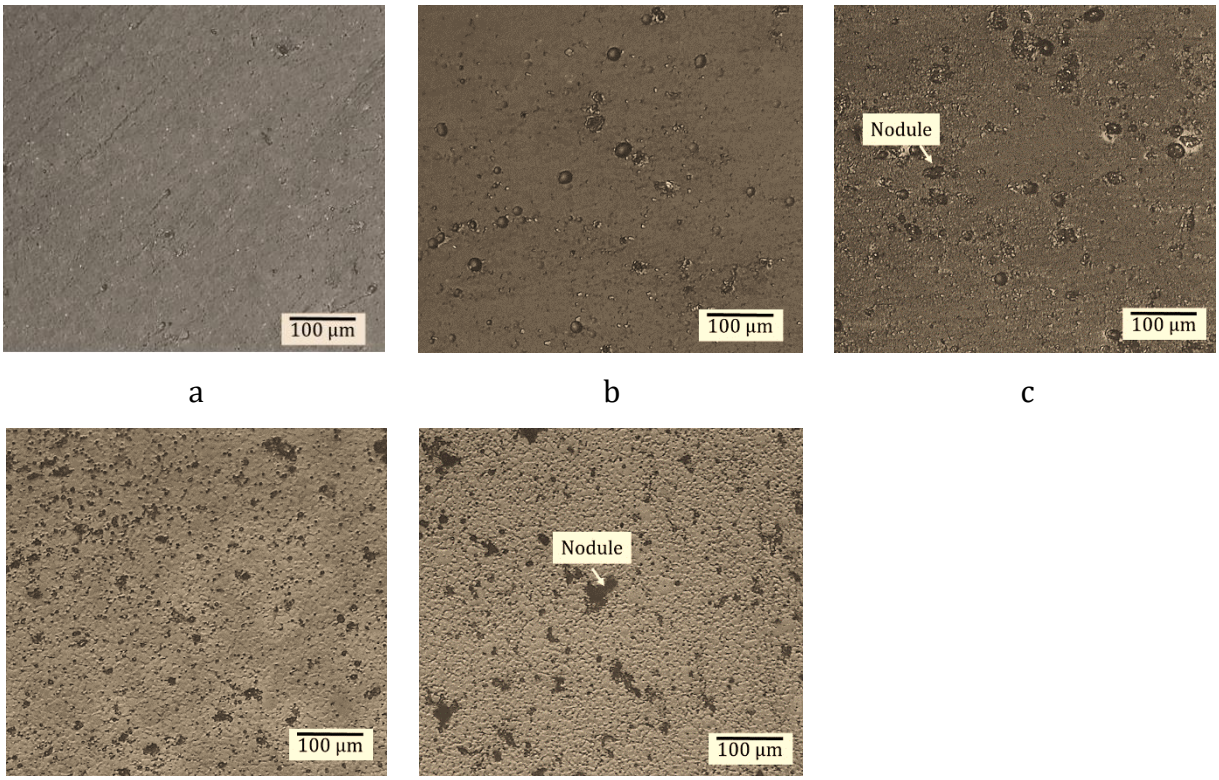

Figure 2 .The OM images of all prepared coatings, including (a) Ni-P, (b) Ni-P-10M-10S, (c) Ni-P-10M-20S, (d) Ni-P-2.5T, and (e) Ni-P-5T

As shown in Figure 1(a), the Ni-P coating showed a uniformed layer with the lowest nodules on the surface. The presence of theses nodules was also reported by other research [7]. When reinforcements (MoS_2, nano-SiO_2, and toner particles) were added to the Ni-P coatings the amount of nodules on the surface of coatings increased. In addition, when the content of toner particles in the bath increased from 1 to 2.5 g/L, the nodules were collected in one

Preprints (www.preprints.org) | NOT PEER-REVIEWED | Posted: 26 October 2020 doi:10.20944/preprints202010.0525.v1

area, as shown in Figure 1(e). It was reported the nodule could affect the properties of coatings since they changed the roughness of coatings [11].

Figure 3 depicts the FESEM images of the surface for three coatings. The presence of nodules is shown obviously on the surface. These nodules showed that the coating deposition was initiated at the preferred regions on the steel substrate, then the lateral development followed by vertical development was done for deposits [2]. When the reinforcement particles were added to the bath, more nodules would be created on the surface. It was found that these particles could provide nucleation sites for the reduction of Ni ions [3]. The large nodules are seen in the white-colored area in the black matrix which found for the Ni-P-2.5T coating. A high magnification FESEM image of one nodule is presented in Figure 3(d). It showed a cauliflower-like structure. This morphology was well-known for electroless Ni-P coatings and was also found in other reports [9, 11]. Thus, based on the presence of reinforcements the smoothness of surface decreased in comparison to the Ni-P coating. Moreover, there were no micro-cracks on the surface of the coatings. It was found that when the deposition technique was electro-plating, the Ni-P coating exhibited micro-cracks and micro-pores [1]. As shown in Figure3(c), for the Ni-P-2.5T coating the nodular lumps were observed. This behavior attributed to the formation of the crystalline nickel phase in the composite coatings [11]. More details of composite coatings microstructure and the energy dispersive X-ray spectrometry (EDS) results were found in other research [7].

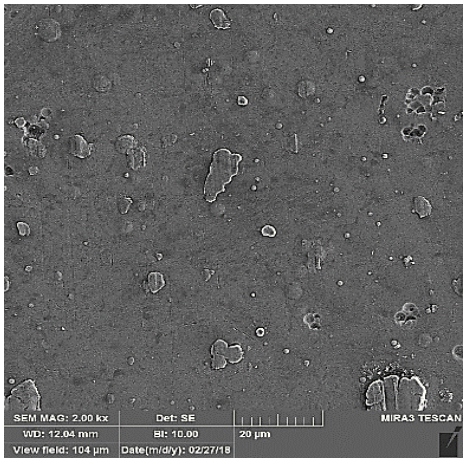

a

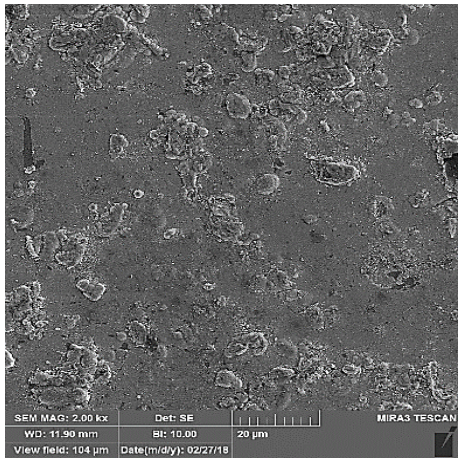

b

Preprints (www.preprints.org) | NOT PEER-REVIEWED | Posted: 26 October 2020 doi:10.20944/preprints202010.0525.v1

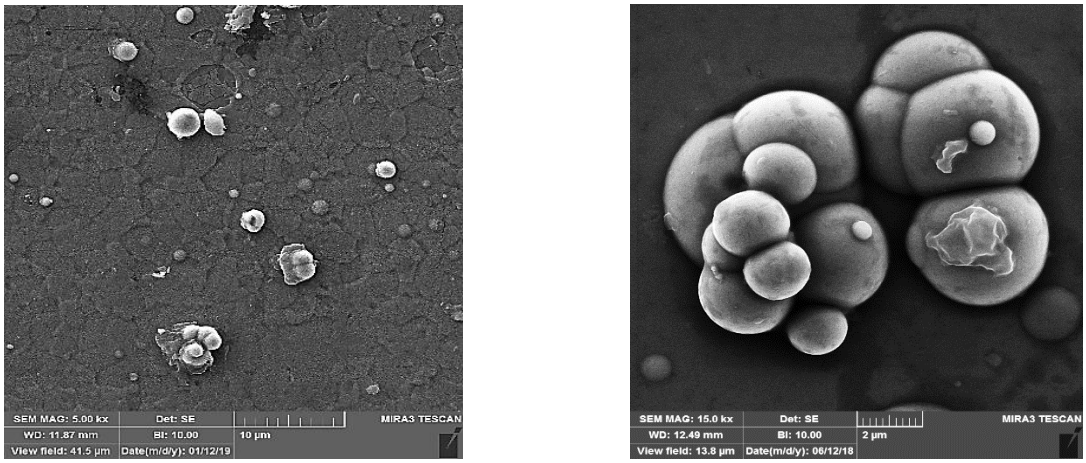

c d

Figure 3. The FESEM images of coatings, including (a) Ni-P, (b) Ni-P-10M-10S, (c) and (d) Ni-P-2.5T

The thickness of all coatings was measured based on the cross-section FESEM images and reported in Table 2. Although the deposition time of all coatings was constant, the deposition rate and the thickness of composite coatings were higher than Ni-P coating. The highest thickness was related to the Ni-P coatings reinforced with toner particles. It was found that the reinforcement particles could be adsorbed on the steel surface and acted as nucleation sites for Ni reduction. Thus, the deposition rate would be increased [7]. Therefore, the presence of reinforcement in the Ni-P bath could affect the thickness of coatings. A similar trend was also reported in other research [23].

Table 2. The measured coatings thickness

Coatings name	Thickness of coating (µm)
Ni-P	4.8 ± 0.1
Ni-P-10M-10S	7.1 ± 0.1
Ni-P-10M-20S	7.0 ± 0.1
Ni-P-1T	13.1 ± 0.1
Ni-P-2.5T	12.0 ± 0.1

Preprints (www.preprints.org) | NOT PEER-REVIEWED | Posted: 26 October 2020 doi:10.20944/preprints202010.0525.v1

3.3. XRD analysis

Figure 4 shows various XRD patterns for different coatings. For the Ni-P coating, the crystalline phases of Ni_3P and Ni were detected. It was noticeable that the Ni-P coating deposited through the electroless method was usually amorphous; however, the heat treating after the deposition process caused to form crystalline phases [7, 2]. The dominated plane for the Ni phase was the plane of (111). It was found that for Ni reduction the following possible reactions would be occurred [25-27]

$2H_2PO_2^- + Ni^+ + 2\ H_2O = 2H_2PO_3^- + 2H^+ + Ni + H_2$

$H_2PO_2^- + Ni^+ + H_2O = HPO_3^{2-} + 3H^+ + Ni$

$2H_2PO_2^- + H_2O = HPO_3^2 + H^+ + 2H_{ads}$, $Ni^+ + 2H_{ads} = 2H^+ + Ni$

For the Ni-P-10M-20S coating, two other phases were found due to the XRD pattern. These phases were MoS_2 and $Ni_{2.82}S_2$. The related peaks for the SiO_2 phase were not detected in these patterns since the utilized SiO_2 particles were the amorphous ones. This behavior was also reported in other research [28]. When the reinforcements were added to the Ni-P coating, the crystalline texture for composite coatings changed as the dominated plane for the preferred growth direction altered. For the Ni-P-2.5T coating, plus the Ni_3P and Ni phases, peaks corresponded to Fe_3O_4, and C phases were found on the related XRD pattern. These changes would be predicted that the corrosion behavior of composite coatings would be changed with respect to the Ni-P coating. Due to the higher intensity of peaks for the Ni-P-2.5T coating, it seemed that more crystalline nickel phase was precipitated in the coating. In addition, Naderi et al. [29] reported other metastable phases such as Ni_5P_2 and $Ni_{12}P_5$ would be detected for the Ni-P coating after the similar heat-treatment step; however, these phases were not found in Figure 4. This was could be attributed to the phosphor content in the Ni-P coating.

Preprints (www.preprints.org) | NOT PEER-REVIEWED | Posted: 26 October 2020 doi:10.20944/preprints202010.0525.v1

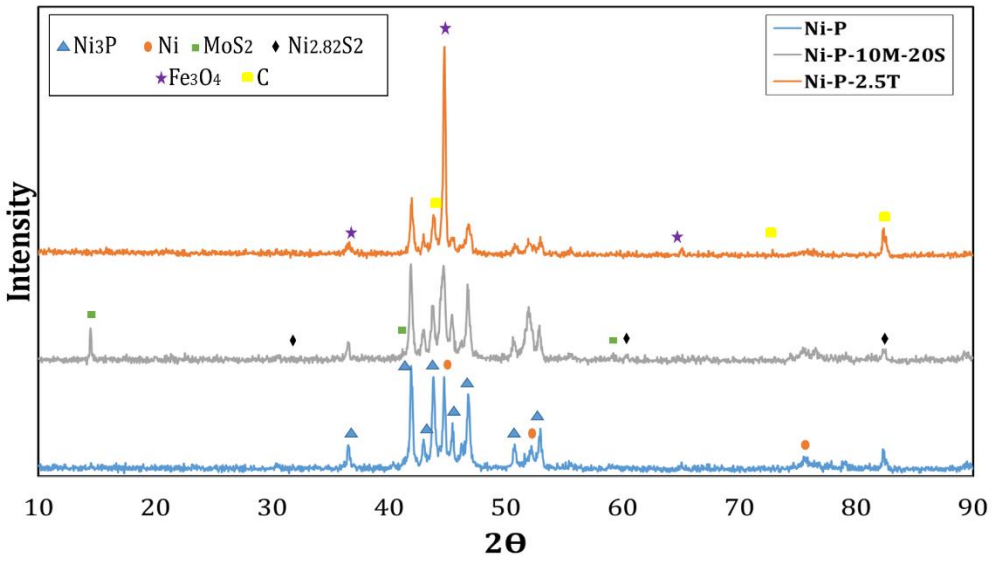

Figure 4. The XRD patterns for various coatings

3.4. Electrochemical test results

Tafel polarization test results for various coatings are shown in Figure 3. Besides, the extracted data of Tafel polarization plots are reported in Table 2.

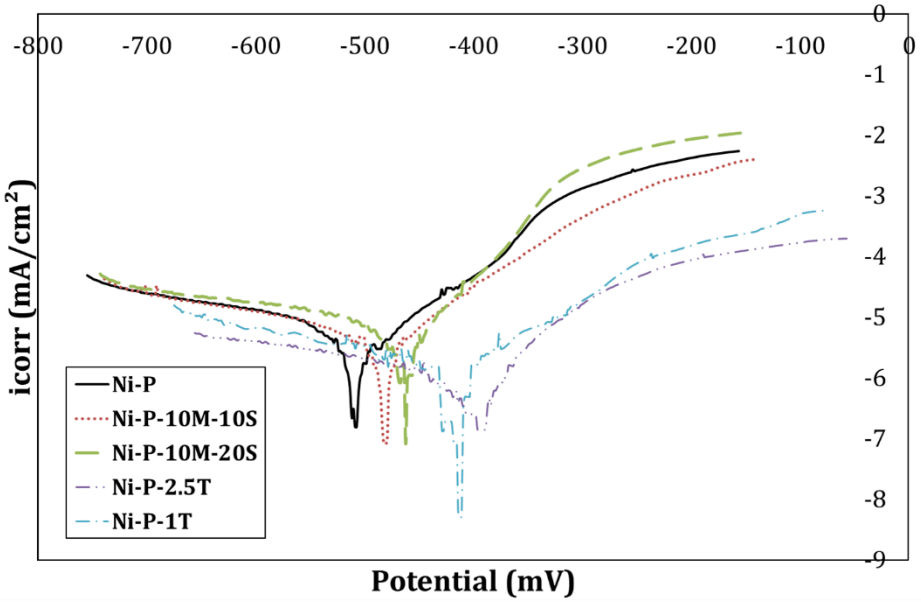

Figure 5. Tafel polarization curves for various coatings in 0.6M NaCl solution

Preprints (www.preprints.org) | NOT PEER-REVIEWED | Posted: 26 October 2020 doi:10.20944/preprints202010.0525.v1

All composite coatings had lower corrosion rates (i_{corr}) in comparison to the Ni-P coating. This reduction was about 22.6 to 91.2%. Changes in the anodic Tafel slope (βa) were more significant with respect to cathodic Tafel slope (βc) when the reinforcements were added to the Ni-P coating. This event showed that the anodic reaction which contained the solution of Ni atom in the corrosive medium ($Ni=Ni^{+2}+2e^{-}$) was obviously affected. The cathodic reaction was the reduction of oxygen ($O_2+H_2O+4e^{-}=4OH^{-}$). When the reinforcements were added to the Ni-P coating the activity of Ni atoms reduced. This event could cause a lower corrosion rate. In this situation, by increasing the content of reinforcement the value of *R* would be increased. Besides, the presence of reinforcements in the matrix resulted in microstructure changes for composite coatings. This behavior could hinder the initiation of corrosion when reinforcements acted as cathode regions and increased the anode polarization [12]. The values of βa and βc for the fabricated coatings were from -38.1 to -202.3 and 20.0 to 49.2 mV/decade, respectively. In addition, the corrosion potential of all composite coatings decreased compared to the Ni-P coating, however, this reduction was more obvious for coatings which contained toner particles. This observation depicted that by changing the chemical composition of coatings, all composite coatings had a lower tendency to corrosion reaction thermodynamically. As shown in Figure 4, various phases detected for composite coatings that affected the value of *E*corr. Therefore, the values of *E*corr for all composite coatings were less negative than the *E*corr for the Ni-P coating. In addition, by increasing the content of reinforcements in the coating, the values of *E*corr became less negative. This observation demonstrated less tendency to the anodic reaction for theses coatings. The range of the *E*corr values for all composite coatings was -520.1-398.3 mV. Similar behavior was also found by other research [13]. Figure 3 shows that there was no obvious passive region for all coatings. This behavior could be related to the roughness of the surface. Toloei et al. [30] reported that high surface roughness usually accelerated the corrosion rate due to the less tendency of surface to create a complete passive layer. Totally, the lowest corrosion rate corresponded to the Ni-P-10M-20S coating. It was noticeable that although composite coatings reinforced by toner particles had the highest thickness, the surface roughness of these coating was also high enough to increase the corrosion rate with respect to other composite coatings. Besides, changes in the texture pattern also led to alterations in the electrochemical behavior of coatings.

Preprints (www.preprints.org) | NOT PEER-REVIEWED | Posted: 26 October 2020 doi:10.20944/preprints202010.0525.v1

Table 2. Data based on Tafel polarization results

Coatings name	i_{corr}(mA/cm^2)	*Ecorr(mV)*	βc (mV/decade)	βa (mV/decade)	*R*
Ni-P	0.0159	-520.1	46.3	-202.3	-
Ni-P-10M-10S	0.0123	-496.7	49.2	-194.7	22.6
Ni-P-10M-20S	0.0014	-483.8	20.1	-62.1	91.2
Ni-P-1T	0.0098	-438.9	20.0	-38.1	38.4
Ni-P-2.5T	0.0020	-398.3	27.8	-40.1	87.4

Figure 4 shows Nyquist and bode plots for various coatings in the corrosive medium after 1 and 24 hours. Due to these plots, the impedance resistance of all composite coatings was higher than the Ni-P coating for both immersion times. Besides, both plots for all coatings with different immersion times showed the same pattern. Similar behavior was also reported by the other study [6]. For a better interpretation of plots a model of electrical circuit was suggested through the Z-view software, as shown in Figure 5. All plots of fabricated coatings were obeyed from this model. This model contained two circuits which attributed to properties of coating for high frequency and the double layer at the interface of coating/ substrate for low frequency. A similar trend was also reported for other Ni-P coatings [31]. Thus, *CPE*f and *R*f were related to the capacity and resistance of coating as a film on the steel substrate, respectively. Besides, *CPE*dl and *R*p were the capacitance and resistance of the double layer that formed at the interface of coating/substrate. In addition, the element of *R*s showed the resistance of the corrosive solution. Data of various elements in the electrical circuit for all coatings after 1 and 24 hours were reported in Tables 3 and 4, respectively. It was found that when there were two separate circuits in the electrical model, two semi-circulars appeared in the Nyquist plot [19, 32]. These semi-circulars was more obvious for the Ni-P-10M-20S coating. It was notable that due to the coating roughness, in the electrical circuit pure capacitive elements were replaced by constant phase elements (*CPE*) [31].

Preprints (www.preprints.org) | NOT PEER-REVIEWED | Posted: 26 October 2020 doi:10.20944/preprints202010.0525.v1

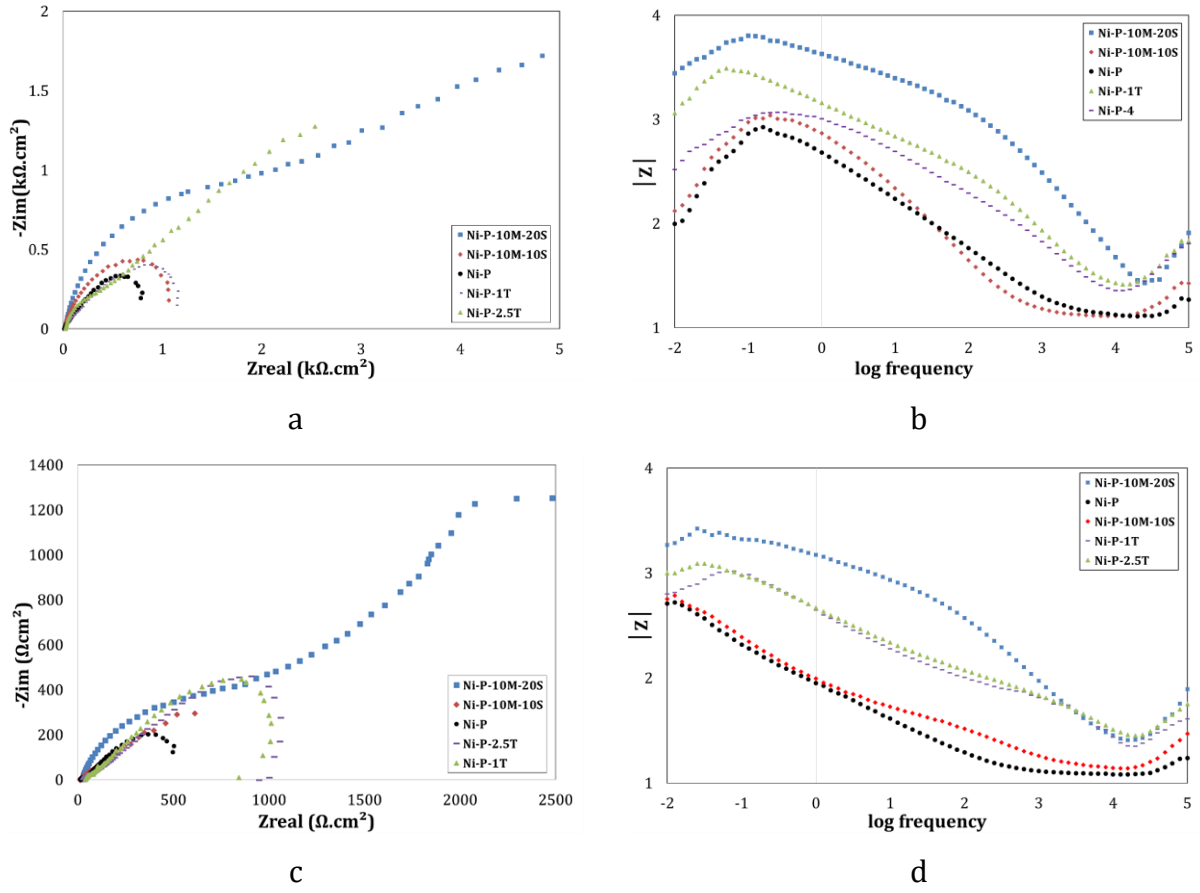

a b c d

Figure 6. Nyquist and bode plots for various coatings (a) and (b) after 1 hour, and (c) and (d) after 24 hours

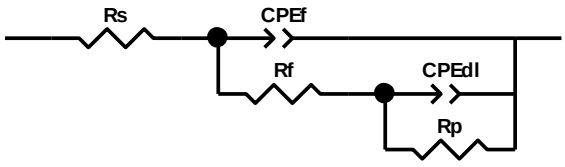

Figure 7. Model of the electrical circuit for EIS plot interpretation

As shown in Table 3, the values of R_f and R_p for all composite coatings were higher than the Ni-P coating. Such behavior depicted that the resistance of these composite coatings against the attack of corrosive ions was higher than the Ni-P coating. This was attributed to the fact that the reinforcement particles would be acted as physical barriers for the diffusion of corrosive ions toward the substrate. This event was shown schematically in Figure 6. When

Preprints (www.preprints.org) | NOT PEER-REVIEWED | Posted: 26 October 2020 doi:10.20944/preprints202010.0525.v1

more reinforcements were added to the Ni-P coating the path of diffusion for corrosive ions toward the steel substrate increased which resulted in an increase in the penetration time. Thus, the increase in the corrosion resistance increased by raising the content of reinforcement in Ni-P coating. In addition, the adsorption of Cl^- ions would be decreased by composite coatings since the utilized reinforcements could act as a dielectric phase. This mechanism was also found in other research [8]. In this situation, composite coatings exhibited higher impedance with respect to the Ni-P coating. Thus, the increase in values of R for various composite coatings was in the range of 18.4 to 85.3% when the immersion time was 1 hour. Besides, the highest of its value was related to the Ni-P-10M-20S coating, similar to results of the Tafel polarization test. Moreover, an increase in the coating thickness in the presence of reinforcements would have resulted in an increase of R_f values when the distance for the diffusion of corrosive ions toward the steel substrate increased. Besides, R_f values for composite coatings contained toner particles were lower than other composite coatings. This event suggested that the adsorption of water and other corrosive ions on these coatings were higher than composite coatings consisted of MoS_2, and nano-SiO_2 particles. In addition, values of CPE_f for all composite coatings were lower than the Ni-P coating. When the CPE_f was high it showed that the area of capacitance was high. This event was related to the increase in the surface roughness resulted from corrosion reactions and nickel dissolution in the corrosive medium [18, 19]. In addition, the dielectric constant which was corresponded to the chemical composition of coating was higher for the Ni-P coating with respect to other coatings. Moreover, values of CPE_{dl} for most composite coatings were lower than the Ni-P coating. This observation showed that lower water molecules and corrosive ions could reach the interface of coating and steel substrates through defects of coatings.

As reported in Table 4, after 24 hours, values for Rs increased insignificantly for all coatings. This increase was attributed to the changes in the amount of corrosive ions in the medium after 24 hours. The value of CPE_{dl} for the Ni-P coating was the highest among other coatings. This behavior would be related to the more adsorption of water molecules on the coating and diffusion of Cl^- ions through defects of coatings. Similar to data in Table 3, values of R_f and R_p for all composite coatings were higher than the Ni-P coating. The range of R values for various composite coatings was about 18.1 to 73.2%. This event depicted that by increasing the immersion time, the value of R would be decreased. Besides, the highest of its value was

Preprints (www.preprints.org) | NOT PEER-REVIEWED | Posted: 26 October 2020 doi:10.20944/preprints202010.0525.v1

attributed to the Ni-P-10M-20S coating. Totally, the presence of all utilized reinforcements was effective to increase the corrosion resistance of the Ni-P coating in 0.6M NaCl solution; however, the average increase for composite coatings reinforced by MoS_2, and nano-SiO_2 particles was more than ones contained toner particles.

Table 3. Extracted data from EIS plots for various coatings after 1 h in 0.6M NaCl solution

Coatings name	R_s (Ω)	R_f (Ω)	CPE_f (μF)	n	R_p(Ω)	CPE_{dl}(μF)	n	R
Ni-P	12.84	107.8	97.4	0.78	889	445.1	0.63	-
Ni-P-10M-10S	13.65	270.4	87.57	0.87	1090	248.7	0.64	18.4
Ni-P-10M-20S	16.04	932.9	2.21	0.91	6042	67.5	0.45	85.3
Ni-P-1T	13.83	120.2	45.17	0.90	1296	474.1	0.62	31.4
Ni-P-2.5T	15.29	534.0	40.54	0.81	2545	574.8	0.69	65.1

Table 4. Extracted data from EIS plots for various coatings after 24 h in 0.6M NaCl solution

Coatings name	R_s(Ω)	R_f (Ω)	CPE_f (μF)	n	R_p(Ω)	CPE_{dl}(μF)	n	R
Ni-P	14.3	43.5	471.5	0.65	682	4531.9	0.63	-
Ni-P-10M-10S	17.2	123.4	217.7	0.59	833	550.1	0.69	18.1
Ni-P-10M-20S	24.1	884.1	8.3	0.82	2543	265.1	0.78	73.2
Ni-P-1T	21.3	85.1	2.9	0.86	893	964.9	0.63	23.6
Ni-P-2.5T	24.4	120.9	68.9	0.76	1173	643.1	0.59	41.8

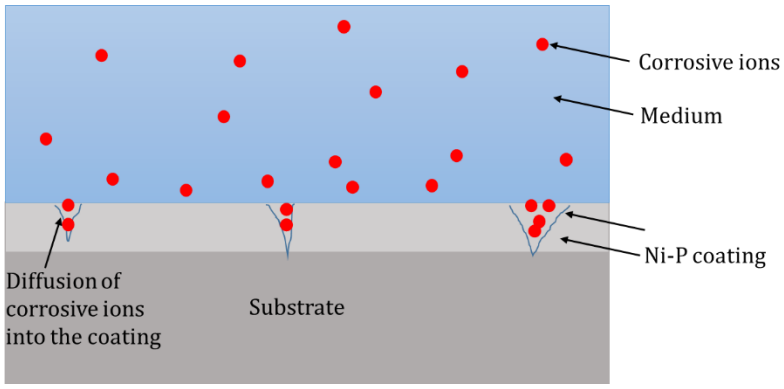

a

Preprints (www.preprints.org) | NOT PEER-REVIEWED | Posted: 26 October 2020 doi:10.20944/preprints202010.0525.v1

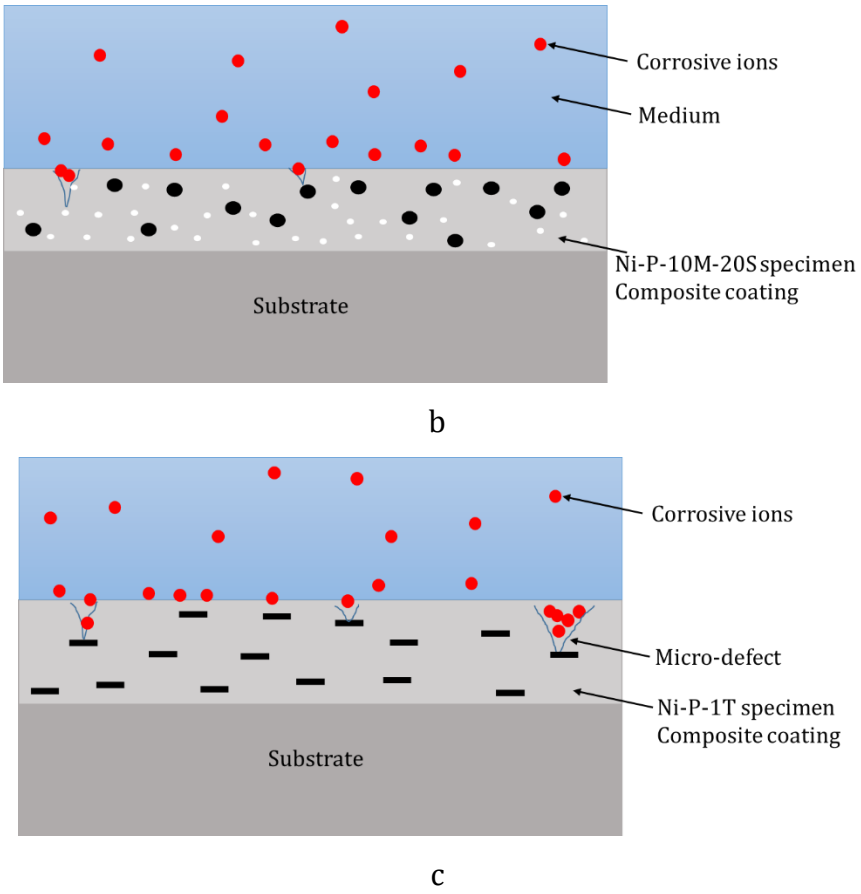

Figure 8. Scheme images of corrosive ion diffusion from solution to various coatings, including, (a) Ni-P, (b) Ni-P-10M-20S and (c) Ni-P-2.5T coatings

Conclusions

In this paper, the electrochemical properties of various electroless Ni-P coatings reinforced by toner, MoS_2, and nano-SiO_2 particles were performed. The obtained results can be summarized as follows:

- FESEM images showed that all coatings exhibited various nodules; however, the composite coatings contained more and larger cauliflower-like nodules. This behavior could be attributed to the presence of reinforcement. In addition, the deposition rate and the thickness of composite coatings increased 2-3 times in comparison to the Ni-P coating.
- The XRD result depicted that all composite coatings would be crystallized when heat tread at 400 ^{o}C for 1 h. All fabricated coatings had Ni and Ni_3P phases, however, the

 doi:10.20944/preprints202010.0525.v1

preferred plane for Ni phase changed for composite coatings. Changes in the texture patterns also caused alterations in the electrochemical behaviors of coatings.

- Tafel polarization results showed that all coatings exhibited lower corrosion rates with respect to Ni-P coatings. The range of this reduction was about 21.6-92.2%. Changes in corrosion properties of composite coatings have corresponded to various detected phases, presence of reinforcement as barriers, and changes in the thickness of the coatings.
- Based on the EIS results, the Ni-P composite coatings showed higher impedance resistance values compared to the Ni-P coating. This increased range was about 18.4-85.3% after 1 h. The two-loop circuit was suggested as an equivalent electrical circuit for all coatings. This event showed similar corrosion mechanisms for all fabricated coatings.
- All utilized reinforcements were effective to increase the corrosion resistance of the Ni-P coating in 0.6M NaCl solution; however, the average increase for composite coatings reinforced by MoS_2, and nano-SiO_2 particles was more than ones contained toner particles. Thus, the highest corrosion resistance was related to the Ni-P-10M-20S coating.

References

[1] Q. Zhou, S. Liu, Y. Zhang, Z. Zhu, W. Su, M. Sheng, Fabrication of porous Cu supported Ni-P/CeO_2 composite coatings for enhanced hydrogen evolution reaction in alkaline solution, Ceramics International 4(6) (2019) 1879-1889

[2] I.S. Thakur, V.S. Pandey, P.S. Rao, S. Tyagi, D. Goyal, Tribological study of mechanically milled graphite nanoparticles codeposited in electroless Ni-P coatings, Metal Powder Report (2020)

[3] M. Czagany, P. Baumli, Effect of surfactants on the behavior of the Ni-P bath and on the formation of electroless Ni-P-TiC composite coatings, Surface and Coatings Technology 361 (2019) 42–49

[4] D. G. Agredo Diaz, A. Barba Pingarron, J. J. Olaya Florez, J. Rafael, G. Parra, J. Cervantes Cabello, I. Angarita Moncaleano, A. Covelo Villar, M. A Hernandez Gallegos, Effect of a Ni-P

coating on the corrosion resistance of an additive manufacturing carbon steel immersed in a 0.1 M NaCl solution, Materials Letters 275 (2020) 128159

[5] A.R. K. Rana, Z. Farhat, Preparation and tribological characterization of graphene incorporated electroless Ni-P composite coatings, Surface and Coatings Technology 369 (2019) 334-346

[6] C. Cui, H. Du, H. Liu, T. Xiong, Corrosion behavior of the electroless Ni-P coating on the pore walls of the lotus-type porous copper, Corrosion Science 162 (2020) 108202

[7] F. A. Eranegh, M. Azadi, H. Tavakoli, Effect of SiO_2 nanoparticles addition on tribological and electrochemical behaviors of Ni–P–MoS_2 multi-component coatings after heat treatment, Surface Engineering and Applied Electrochemistry, 56(2) (2020) 171-183

[8] M. S. Safavi, A. Rasooli, Ni-P-TiO_2 nanocomposite coatings with uniformly dispersed Ni_3Ti intermetallics: Effects of current density and post heat treatment, Surface and Coatings Technology 372 (2019) 252-259

[9] B. Chen, J. Guo, M.F. Yan, F. Wang, F. Liu, Study on a Ni-P-nano TiN composite coating for significantly improving the service life of copper alloy synchronizer rings, Applied Surface Science 504 (2020) 144116

[10] D. Ram Dhakal, G. Gyawali, Y.K. Kshetri, J. H. Choi, S. W. Lee, Microstructural and electrochemical corrosion properties of electroless Ni-P-TaC composite coating, Surface and Coatings Technology (2020)

[11] A.R. Shashikala, B.S. Sridhar, Codeposition of electroless Ni-P/ZnO nano composites and evaluation of corrosion resistance of the coatings, Materials Today: Proceedings (2020)

[12] Y. Du, X. Zhang a, L. Wei, B. Yu, Y. Wang, Y. Wang, S. Ye, Electrodeposition of a Ni-P composite coating reinforced with $Ti_3C_2T_x$@TiO_2/MoS_2 particles, Materials Chemistry and Physics 241 (2020) 122448

[13] A. Sharma, A. K. Singh, Corrosion, and wear study of Ni-P-PTFE-Al_2O_3 coating: the effect of heat treatment, Central European Journal of Engineering 4(1) (2014) 80-89

[14] Y. Wu, L. Liu, B. Shen, W. Hu, Study of self-lubricant Ni-P-PTFE-SiC composite coating, Journal of Materials Science 40 (15) (2005) 5056-5059

[15] L. Ping, Z. Yongwei, Z. Gaoyan, Z. Xiao, W. Shuncai, Y. Shoufeng, Surfactant-free electroless codeposition of Ni-P-MoS_2/Al_2O_3 composite coatings, Coatings 9 (2) (2019) 116

[16] F. Mayanglambam, M. Russell, Reusing oxide-based pulverised fly ash and medical waste particles to develop electroless nickel composite coatings (Ni-P/fly ash and Ni-P/SiO_2-Al_2O_3) International Journal of Minerals, Metallurgy and Materials 27(2020) 1147–1156

[17] P. Nezhadi, M. Azadi, M. Shojaie Bahaabad Effects of toner particles addition on fabrication and characterizations of aluminum oxide layers, Surfaces and Interfaces 18 (2020) 100450

[18] M. Azadi, M.J. Olya, M.E. Bahrololoom, EIS study of epoxy paints in two different corrosive environments with a new filler: rice husk ash, Progress in Color, Colorants, and Coatings 9(1) (2016) 53-60

[19] M. Azadi, M Ferdosi Heragh, M.A. Bidi Electrochemical characterizations of epoxy coatings embedded by modified calcium carbonate particles, Progress in Color, Colorants, and Coatings 13(4) (2020) 213-222

[20] F. Ahangaran, A. Hassanzadeh, S. Nouri, Surface modification of Fe_3O_4@SiO_2 microsphere by silane coupling agent, International Nano Letters 3 (2013) 23

[21] M. A. Bidi, M. Azadi, M. Rassouli, A new green inhibitor for lowering the corrosion rate of carbon steel in 1 M HCl solution: Hyalomma tick extract, Materials Today Communications 24 (2020) 100996

[22] N. Verma, R. Kumar, V. Sharma, Analysis of laser printer and photocopier toners by spectral properties and chemometrics, Spectrochimica Acta Part A: Molecular and Biomolecular Spectroscopy 196 (2018) 40-48

[23] L. Yan, Y. S.Rong, L. J.Dan, H. Z.Wu, Y. D. Sheng, Microstructure and wear resistance of electrodeposited Ni-SiO_2 nano-composite coatings on AZ91HP magnesium alloy substrate, Transaction of Nonferrous Metal Society of China 21 (2011)483-488

[24] S. Touri, S.M. Monirvaghefi, Fabrication and characterization of functionally graded Ni-P electroless coating with variable properties along the surface of the coating, Materials Today Communications 24 (2020) 101203

[25] A. Stankiewicz, Z. Kefallinou, G. Mordarski, Z. Jagoda, B. Spencer, Surface functionalisation by the introduction of self-healing properties into electroless Ni-P coatings, Electrochimica Acta 297 (2019) 427-434

[26] Z. Sharifalhoseini , M. H. Entezari, A. Davoodi, M. Shahidi, Access to nanocrystalline, uniform, and fine-grained Ni-P coating with improved anticorrosive action through the

growth of ZnO nanostructures before the plating process, Corrosion Science 172 (2020) 108743

[27] J.D. Lin, C.T. Chou, The influence of phosphorus content on the microstructure and specific capacitance of etched electroless Ni-P coatings, Surface and Coatings Technology 368 (2019) 126-137

[28] M. Mollaei, M. Azadi, H. Tavakoli, A parametric study on mechanical properties of aluminum–silicon/SiO_2 nano-composites by a solid–liquid phase processing, Applied Physics A 124 (7) (2018) 504

[29] J. Naderi, A. A.D. Sarhan, Measure and evaluate the hardness of the electrodeposited Nickel-Phosphorous (Ni-P) thin film coating on carbon steel alloy for automotive applications, Measurement 139 (2019) 490-497

[30] A. Toloei, V. Stoilov, D. Northwood, The relationship between surface roughness and corrosion, ASME 2013 International Mechanical Engineering Congress and Exposition vol. 2B, Advanced Manufacturing, 2013

[31] F.F. Marzo, M. Alberro, A.P. Manso, X. Garikano, C. Alegre, M. Montiel, A. Lozano, F. Barreras, Evaluation of the corrosion resistance of Ni(P)Cr coatings for bipolar plates by electrochemical impedance spectroscopy, International Journal of Hydrogen Energy 45(40) (2020) 20632-20646

[32] M. Arab, M. Azadi, O. Mirzaee, Effects of manufacturing parameters on the corrosion behavior of Al-B_4C nanocomposites, Materials Chemistry and Physics 253 (2020) 123259